



Control of the sharkskin instability in the extrusion of polymer melts using induced temperature gradients

Erik Miller
Department of Mechanical Engineering
University of Massachusetts
Amherst, MA 01003-2210, USA

Introduction

Flow instabilities occur in a variety of commercial polymer processing operations including extrusion, film blowing, fiber spinning and coating. During the extrusion of molten polymer through capillary or slit die geometries, a transition from a smooth surface to a nearly periodic ridge-like surface distortion has been observed at a critical shear rate or wall shear stress [1, 2]. These surface distortions are known as sharkskin. Flow instabilities during extrusion were first observed after World War II, and early reports of sharkskin, in particular, date to the 1960's [3, 4]. Detailed experimental observations on flow instabilities through 1975 have been reviewed in a broad sense [1, 2, 5]. In general, and as detailed in the aforementioned reviews, distortions seen during extrusion have a progression in severity. As shear rate or stress increases, the extrudate surface undergoes a transition from stable, to sharkskin, to stick-slip, and finally to gross melt fracture.

While a great deal of research has been devoted to sharkskin in polymer extrusion, the origins and underlying physical mechanism of this elastic instability are still widely debated within literature. There is, however, a consensus among researchers that the underlying physical mechanism of the sharkskin instability is rooted in the kinematics and dynamics of the flow near the capillary die exit and the build up of tensile stress resulting from the stress singularity that develops at the die exit [6-9]. Experiments have been performed in which the effects of the exit corner were explicitly probed. Sharkskin has been suppressed or completely eliminated using dies that have been dipped or coated in slip-inducing fluoroelastomer additives [10, 11], and even simple soap solutions [12]. Although successful, additives are not always desirable in a final product and, therefore, die material alternatives have also been explored. These include special stainless steel dies with Teflon™ inserts [13] and dies constructed from alpha brass [14-16]. Another strategy is that of using temperature to control or eliminate flow instabilities by decreasing viscosity; both die heating [17, 18] and cooling [6, 19, 20] have been explored.

Problem

Surface quality is important in most extrusion applications. For example, extruded optical fibers must be free from surface defects if they are to transmit light effectively. Thin fibers which are to be woven into some other final product are difficult to work with if their surface is not smooth and able to slide past other fibers easily. Furthermore, although it does not occur with all polymers, sharkskin is prevalent in linear polyethylenes, HDPE and LLDPE, which are some of today's most commonly extruded polymers. Therefore, suppression or elimination and understanding of sharkskin have practical relevance in that the instability limits the output rate for commercially acceptable extrudate.

Rather than addressing the onset of sharkskin by changing the material at the polymer/die interface, our research focuses on affecting the properties of the polymer itself towards the goal of reducing polymeric stress and deformation at the die exit. By using very specific and localized heating/cooling in the die, we will show that it is possible to locally affect the fluid temperature and therefore fluid rheology only near the capillary wall. The rheological properties of polymers are very sensitive in general to small changes in temperature. The theory of time-temperature superposition allows one to relate changes of viscosity and relaxation time to changes in temperature [21]. Specifically, the Arrhenius form of the time-temperature superposition shift factor (valid for polymer melts far from their melting point) suggests that there can exist a strong coupling between flow kinematics and the temperature gradients imposed upon the flow through the thermal boundary conditions such as die heating/cooling [22]. In addition, the relatively poor thermal

conductivity of polymer melts results in the effects of die heating being isolated to the polymeric fluid near the wall and die exit, where it is most critical to the mechanism of the sharkskin instability.

Heating the final section of a capillary die some percent above the bulk working temperature will result in a radial temperature profile in the polymer melt across the plane of the die exit. This profile will vary from some bulk temperature at the centerline to the elevated capillary wall temperature. If the localized heating is designed correctly, the majority of the polymer melt in the resulting temperature distribution will be near the upstream bulk temperature. Consequently, this induced temperature profile will translate into an analogous distribution of the fluid rheology, resulting in a dramatic reduction in both the viscosity and the relaxation time of the polymeric fluid near the die wall. It is our hypothesis that this local modification of the fluid rheology will directly correspond to a respective increase in a critical output rate before the onset of sharkskin.

With respect to all the previous research, our approach to die heating/cooling will utilize a very precise experimental design to locally affect the extrudate at the die exit allowing us to not only suppress sharkskin, but also quantify its characteristics and eventually control and predict it. Practical relevance of our work points to an extrusion method that uses a small amount of added energy in the form of localized die heating to increase output while minimizing necessary bulk temperatures and subsequent cooling times.

Methods

A series of experiments were carried out using a purpose built extruder. In Figure 1, a schematic diagram of our experimental setup highlighting several key components and heating zones is shown. The barrel, with a 30mm internal diameter and total volume of 0.19m³, was machined from 7075 aluminum and heated by three 500W band heaters (Omega MB-1). Temperature of the bulk fluid inside the barrel (Zone 3) is monitored by an internal bore thermocouple (Omega BT) inserted through a radial pressure fitting near the bottom of the barrel. A standard pipe fitting provides the attachment point for the intermediate and capillary die, both constructed of stainless steel and heated by a 100W band heater (Omega MB-1) and 15W cartridge heater (Omega CSS-01115), respectively. In the intermediate die (Zone 2), bulk temperature of the fluid is again monitored by an internal bore thermocouple. However, in the capillary die (Zone 1), the temperature of the die itself is monitored by a surface mount thermocouple. A divider fabricated from Teflon provides thermal isolation to the small capillary die. Temperature differences of $\Delta T > 30^{\circ}\text{C}$ are possible between the capillary and intermediate die. The actual capillary section begins in the intermediate die and is bored smoothly through the 3mm thick Teflon™ gap and the 5mm capillary die. Total length is 10mm and diameter is 2mm ($L/D = 5$). All three heating zones are controlled individually by standard proportional-integral controllers (Omega CN2110). Polymer melt is forced out of the barrel and through the die using pressurized nitrogen supplied with a standard compressed nitrogen tank and regulator capable of producing $1.4 \times 10^7 \text{ Pa}$. The regulated pressure is monitored by a 100mV transducer (Omega PX302) mounted inline at the top of the barrel.

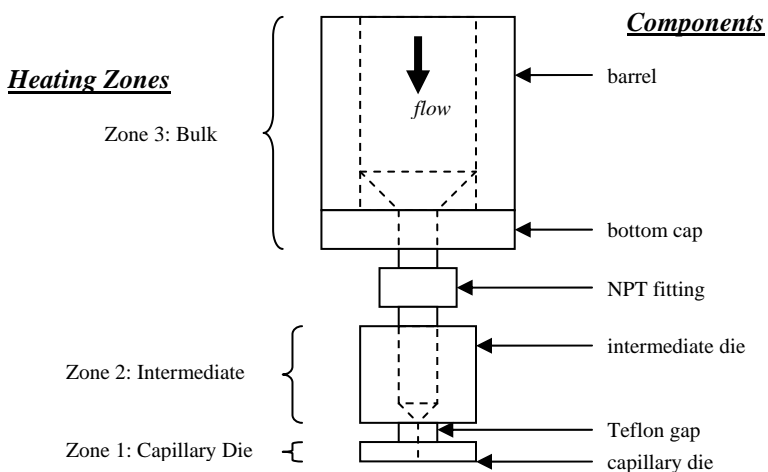


Figure 1: Schematic diagram of experimental extruder.

Temperature differences of $\Delta T > 30^{\circ}\text{C}$ are possible between the capillary and intermediate die. The actual capillary section begins in the intermediate die and is bored smoothly through the 3mm thick Teflon™ gap and the 5mm capillary die. Total length is 10mm and diameter is 2mm ($L/D = 5$). All three heating zones are controlled individually by standard proportional-integral controllers (Omega CN2110). Polymer melt is forced out of the barrel and through the die using pressurized nitrogen supplied with a standard compressed nitrogen tank and regulator capable of producing $1.4 \times 10^7 \text{ Pa}$. The regulated pressure is monitored by a 100mV transducer (Omega PX302) mounted inline at the top of the barrel.

The material under investigation is a polyolefin plastomer, specifically, a co-polymer of ethylene and octene. Dow AFFINITY™ EG8100 was chosen on the basis of being a well-stabilized and commercially available linear low-density polyethylene (LLDPE) [11]. The density of this polymer is $\rho = 870 \text{ kg/m}^3$, and it has a differential scanning calorimeter (DSC) melting point of $T_{melt} = 55^{\circ}\text{C}$. EG8100 was delivered in pellet form and, in the absence of any instability, is almost completely transparent. Dynamic and steady flow rheology

Table 1: Spectrum of relaxation times and moduli

Relaxation Time, λ	Viscosity, η
[s]	[Pa]
1.98×10^{-3}	3.94×10^5
1.24×10^{-2}	2.11×10^5
5.64×10^{-2}	1.19×10^5
0.327	3.24×10^4
3.22	5.07×10^3

experiments were performed on this material using parallel plate geometry on an AR2000 shear rheometer (TA Instruments), the results of which are shown in Figures 2 and 3, respectively. The small amplitude oscillatory data in Figure 2 were fit using a discrete multi-mode Maxwell spectrum [21]. A satisfactory fit was produced with 5 modes; the relaxation times, λ_i , and viscosities, η_i , associated with each mode are given in Table 1; the model predictions are superimposed over the data in Figure 2. An average or Oldroyd relaxation time of $\bar{\lambda} = 1.52\text{s}$ was determined through a viscosity weighted average of the relaxation time spectrum.

Shifting of the linear viscoelasticity data over a range of temperatures using the Arrhenius form of the time-temperature superposition shift factor allowed for the determination of the activation energy, $\Delta H/R = 3460\text{K}$, which was used in later calculations. The results of fitting the steady shear viscosity data at a reference temperature of 140°C with a Carreau model [21] are superimposed over the data in Figure 3. Using this model,

$$\frac{\eta - \eta_\infty}{\eta_0 - \eta_\infty} = [1 + (\tau_c \dot{\gamma})^2]^{\frac{n-1}{2}}, \quad (1)$$

resulted in a zero-shear rate viscosity of $\eta_0 = 4.0 \times 10^4 \text{Pa}\cdot\text{s}$, an infinite-shear rate viscosity of essentially zero, a time constant for the onset of shear thinning of $\tau_c = 24\text{s}$, and a power law exponent of $n = 0.83$. The Carreau model predictions are in good agreement with the viscosity measurements over the entire range of shear rates.

The extruder was initially calibrated by generating flow curves, several of which will be presented in the following sections. Pressure drop, controlled via the regulator on the nitrogen tank, was ramped up while the mass flow rate of extruded polymer was measured. The latter was done by weighing timed samples of extrudate, using an accurate balance with a sensitivity of 0.001g (Mettler AC100), collected at a constant

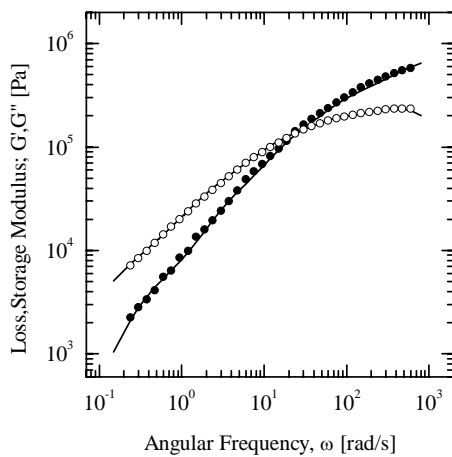


Figure 2: Small amplitude oscillatory shear rheology of EG8100 at $T_{ref} = 140^\circ\text{C}$. The data include: 'o', loss modulus (G''); '•', storage modulus (G'); and '—', fits of a multi-mode Maxwell model, the parameters of which are listed in Table 1.

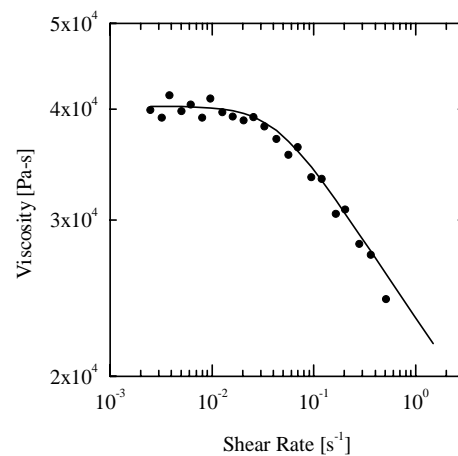


Figure 3: Steady shear rheology of EG8100 at $T_{ref} = 140^\circ\text{C}$. The data include: '•', viscosity measurements; and '—', fit to a Carreau model.

pressure drop. Flow curves were generated at various temperature conditions, where bulk temperature is controlled in zones 2 and 3, and die heating or cooling is done with precise control at Zone 1. We will show through temperature measurements that this precise control affects only a very small portion of the polymer melt near the capillary wall as it exits the die.

Temperature profile measurements of the extrudate were performed using a micro-positioning stage adapted to hold a K-type thermocouple junction at the end of a horizontally oriented protection tube. The exposed junction was marched across the exit plane of the capillary die. The center of the thermocouple junction was aligned to be tangent with the exit plane of the capillary, resulting in no upstream effects within the capillary but still capturing the temperature of the extrudate directly at the exit plane. The thermocouple junction had a diameter of $D_{tc} = 0.35\text{mm}$, resulting in a spatially averaged temperature measurement of the polymer melt. These measurements are invasive and although great care is taken in positioning so the effect is completely downstream of the die exit plane, they can affect the flow as we are trying to measure it. Future experiments are planned with a non-invasive temperature measurement technique known as Dual Emission Laser Induced Fluorescence (DELIF) [23]. These temperature measurements served to confirm the thermal gradient between the extrudate centerline and wall temperature.

Qualitative flow visualization of the extrudate upon exiting the die was done using a CCD camera (Hitachi KP-M22N) and video zoom microscope lens with an increased depth of field (Edmund VZM 450i). Quantitative characterization of the extrudate surface showing the sharkskin instability was done optically. Still images of cooled extrudate samples were taken from frames captured with a CCD camera mated to a microscope (Olympus Vanox-T). Using backlighting, the profile of the extrudate was captured and processed using an edge detection routine we developed in MATLAB™. The routine utilized a max/min function and fast-Fourier transform to calculate the average amplitude and dominant wavelength of the nearly periodic sharkskin profile.

Results and Discussion

We begin our study of thermal modification by acquiring flow curves at various bulk temperatures, as well as die heating and cooling conditions. In Figure 4, the effect of changing the bulk material temperature and comparative lack of effect through die heating or cooling is shown. In the figure, the difference in material properties resulting from a 20°C bulk temperature difference is evident by the increased flow rate for a given

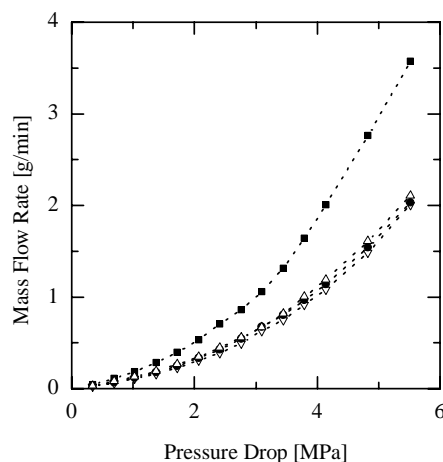


Figure 4: Flow curves showing effects of bulk temperature v. die heating/cooling. The data include: '■', $T_{bulk} = T_{die} = 160^\circ\text{C}$; '●', $T_{bulk} = T_{die} = 140^\circ\text{C}$; '△', die heating - $T_{bulk} = 140^\circ\text{C} / T_{die} = 160^\circ\text{C}$; and '▽', die cooling - $T_{bulk} = 140^\circ\text{C} / T_{die} = 130^\circ\text{C}$.

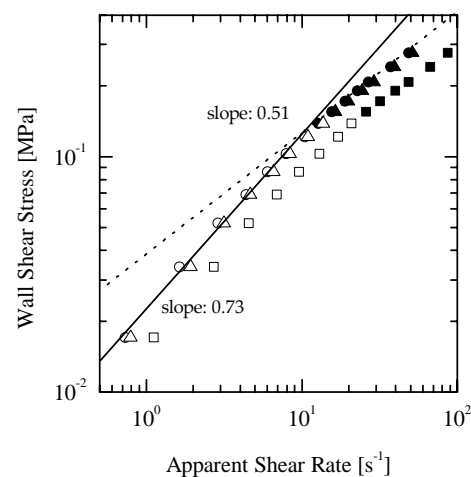


Figure 5: Flow curves showing transition from stable (open symbols) to unstable sharkskin (closed symbols) extrudate. The data include: '○', $T_{bulk} = T_{die} = 140^\circ\text{C}$; '△', $T_{bulk} = 140^\circ\text{C} / T_{die} = 160^\circ\text{C}$; and '□', $T_{bulk} = T_{die} = 160^\circ\text{C}$.

applied pressure drop. As the bulk temperature is increased from $T_{bulk} = 140^{\circ}\text{C}$ to 160°C , the viscosity, calculated using the Arrhenius form of time-temperature superposition for zero-shear, is reduced from $\eta_0 = 4.0 \times 10^4 \text{Pa}\cdot\text{s}$ to $\eta_0 = 2.7 \times 10^4 \text{Pa}\cdot\text{s}$. This 32% decrease in viscosity results in an average 58% increase in mass flow rate, \dot{m} , at a given pressure drop, ΔP . This agrees well with the observations of similar work by Pudjijanto and Denn [24]. In contrast to changing the bulk temperature, the addition of die heating or cooling to the experiment at $T_{bulk} = 140^{\circ}\text{C}$ produces a negligible effect on the flow curve. Thus, although the die is being heated to $T_{die} = 160^{\circ}\text{C}$ or cooled to $T_{die} = 130^{\circ}\text{C}$, these experiments clearly show that only the very outermost polymer melt in the die is being heated or cooled beyond the centerline temperature while the bulk properties of the fluid remain unaffected. These qualitative observations of the localization of our thermal modifications will be reinforced with precise temperature profile measurements.

Utilizing the fact that extruded polyethylene becomes cloudy, or experiences loss of gloss as it transitions to sharkskin, the flow curves can be used to explore the onset of the instability. By qualitatively selecting a critical onset point, the data can be separated into stable and unstable flow regimes. When the data are plotted on a log-log scale, they demonstrate a clear transition in slope upon onset of the surface instability, as seen in Figure 5. Initially, the wall shear stress is found from our experiments to increase exponentially with a slope of 0.7, independently of bulk or wall temperature. However, a clear transition occurs in the data at larger shear rates and the wall shear stress is found to increase with a slope of 0.5, again, independently of wall or bulk temperature. This change of slope coincides precisely with the loss of gloss of the filament and the transition from the stable flow regime to the sharkskin instability. It should be noted that the onset of sharkskin to this point is assessed in a qualitative manner. As we will discuss below, in order to quantify the effectiveness of die heating or cooling, an exacting procedure must be developed to determine the character of the sharkskin instability.

In addition to showing a clear change in slope at the onset of the sharkskin instability, the data in Figure 5 strongly supports our original hypothesis, in that the sharkskin instability can be suppressed through controlled die heating. The three curves shown are extrusion at $T_{bulk} = 140^{\circ}\text{C}$ with no die heating, $T_{bulk} = 140^{\circ}\text{C}$ with die heating to $T_{die} = 160^{\circ}\text{C}$, and $T_{bulk} = 160^{\circ}\text{C}$ with no die heating. It should be noted that no die heating means that the die was controlled at the same temperature as the selected bulk. As in the previous flow curves, the curves for $T_{bulk} = 140^{\circ}\text{C}$ with and without die heating are uniform in terms of stress and shear rate trends. However, the onset point of sharkskin has been suppressed to the next higher experimentally imposed stress level. By heating only the final die exit to $T_{die} = 160^{\circ}\text{C}$ while keeping the bulk temperature at $T_{bulk} = 140^{\circ}\text{C}$, the critical shear stress for the onset of the sharkskin instability, $\tau_{crit} = 0.138 \text{MPa}$, is found to be consistent with the value observed for the experiments where both the bulk and die were heated to $T_{bulk} = T_{die} = 160^{\circ}\text{C}$, albeit at a lower output rate.

In order to quantify the effects of die heating on the polymer melt, temperature measurements were taken at the die exit. In Figure 6, profiles taken at a bulk temperature of $T_{bulk} = 140^{\circ}\text{C}$ with die heating to $T_{die} = 160^{\circ}\text{C}$ at several increasing output rates are shown. The data do not continue to the die exit ($r = 1.0 \text{mm}$) due to the offset caused by the size of the thermocouple junction, $D_{tc} = 0.35 \text{mm}$, in relation to the capillary with diameter, $D = 2 \text{mm}$. As a result of the thermocouple junction being fully submerged in the extrudate at the outermost reading, this offset roughly corresponds to one radius, $R_{tc} = 0.18 \text{mm}$. The measurements correspond to average temperatures across the thermocouple junction which is carefully traversed through the extrudate, tangent to the exit plane of the die. A rough extrapolation of the temperature profiles to the edge of the polymer melt extrudate results in a wall temperature of very close to the applied $T_{die} = 160^{\circ}\text{C}$. At low output rates and small Peclet numbers, the polymer melt has a long

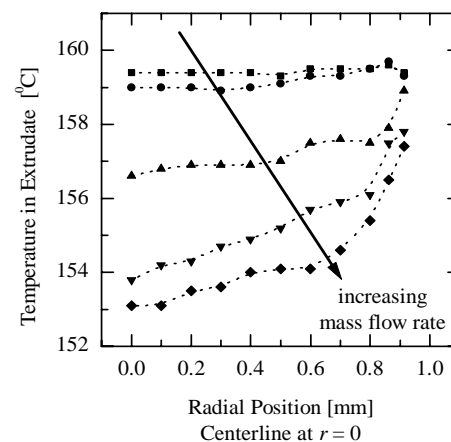


Figure 6: Radial temperature profiles through extrudate across die exit plane for several increasing mass flow rates, from $\dot{m} = 0.079 \text{g/min}$ to $\dot{m} = 1.2 \text{g/min}$.

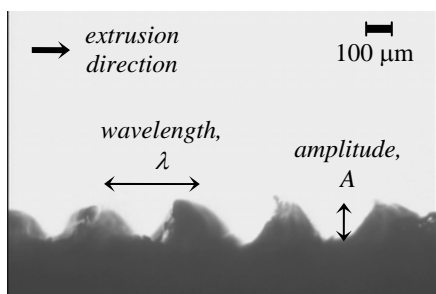


Figure 7: Characteristic profile photo of EG8100 extrudate with fully developed sharkskin surface.

enough residence time in the capillary to be heated to the elevated temperature across the entire profile. As the output rate increases and residence time decreases, a strong temperature gradient develops, isolated near the die wall, and less heat is transferred into the polymer. In lieu of the more precise and non-invasive temperature measurements proposed in the experimental protocol for future work, we can conclude that the stated goal of imposing large temperature gradients on the polymer melt extrudate has been attained.

A still image of an extrudate in profile exhibiting highly developed sharkskin is shown in Figure 7. This image illustrates the parameters we will be using to discuss the nearly periodic nature of the sharkskin instability.

Qualitative visual inspection of extrudate surfaces indicated that sharkskin amplitude and wavelength both increased as output rate increased. The nature of the surface variations was quantified by analyzing images from a wide range of output rates and heating conditions. The resulting plot, seen in Figure 8, is a quantitative processing map of the sharkskin instability. Looking at the instability in terms of the amplitude of the surface roughness, A , there is a clear exponential growth as output rate increases. Furthermore, throughout the range of die heating and cooling conditions tested, this growth rate appears to be consistent. A specific scaling will be discussed in a later section. Preliminary fitting of the data is included in Figure 8 to illustrate uniformity of the data between temperature conditions in the given window. This scaling suggests that the consistent fit is valid for shear rates far from the onset conditions of sharkskin; the initial growth from submicron roughness and smooth surfaces to sharkskin is much stronger. The scatter in the data is due primarily to the $1\mu\text{m}$ resolution of the images used.

There is a need to quantify the onset conditions of the sharkskin instability. Rather than qualitatively assigning a surface as stable or unstable based on its 'by eye' visual appearance, the map shown in Figure 8 allows a specific characteristic amplitude to be designated as the condition for the onset of the sharkskin instability. The quantitative map encompasses the region of processing at the point where some level of instability is already present. This is due to the fact that the optical edge detection routine has difficulty processing amplitudes smaller than about $1\mu\text{m}$. Sharkskin has historically been identified as a loss of gloss on the surface of the extrudate. Based on our qualitative inspection, this corresponds to a surface roughness of approximately $10\mu\text{m}$. If a vertical slice is taken through the data, thereby holding the shear rate fixed, the amplitude is found to decrease as the degree of die heating is increased. This can be seen explicitly in the series of images presented in Figure 9. These images show a decrease in surface roughness from $A = 90\mu\text{m}$ to $25\mu\text{m}$ to $9\mu\text{m}$ as the capillary die wall temperature is decreased from $T_{die} = 170^\circ\text{C}$ to 150°C to 130°C at a shear rate of 30s^{-1} and a bulk temperature of $T_{bulk} = 140^\circ\text{C}$. Thus, a surface temperature modification of 40°C about the bulk temperature produces an order of magnitude difference in the measured sharkskin amplitude. Alternatively, a given amplitude can be selected and a horizontal slice taken through the data in Figure 8. We observe that modification of the die temperature,

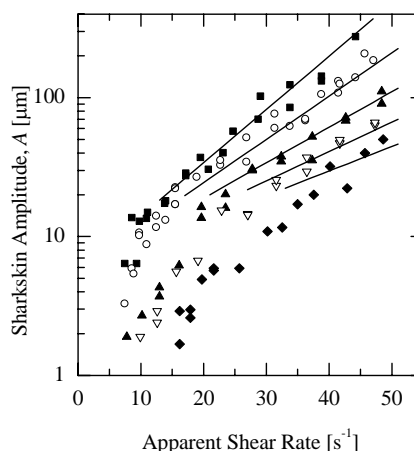


Figure 8: Sharkskin amplitude as a function of shear rate at various die heating or cooling conditions, a quantitative processing map. All curves are at $T_{bulk} = 140^\circ\text{C}$ with die heating/cooling. The data include: '■', $T_{die} = 130^\circ\text{C}$; '○', $T_{die} = 140^\circ\text{C}$; '▲', $T_{die} = 150^\circ\text{C}$; '▽', $T_{die} = 160^\circ\text{C}$; and '◆', $T_{die} = 170^\circ\text{C}$. Exponential fits included and addressed in Figure 12.

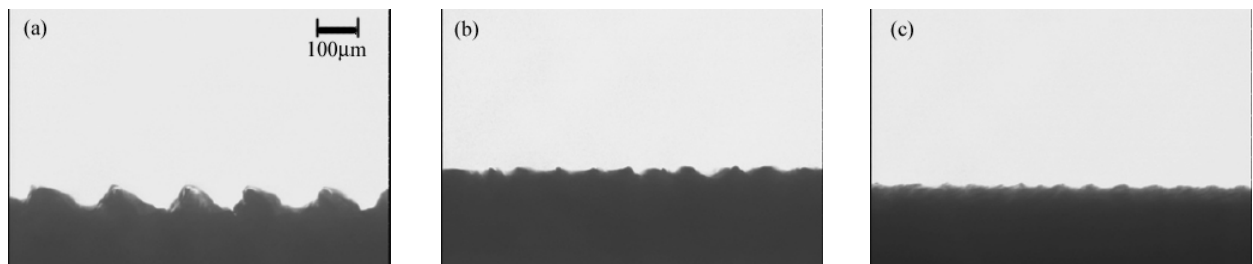


Figure 9: Succession of profile photos at constant apparent shear rate of $\dot{\gamma} = 30s^{-1}$ and a constant bulk temperature of $T_{bulk} = 140^{\circ}C$ with increasing die temperature. The data include: (a) $T_{die} = 130^{\circ}C$, (b) $T_{die} = 150^{\circ}C$, and (c) $T_{die} = 170^{\circ}C$.

again, by $40^{\circ}C$ through localized heating or cooling, makes it possible to change the output rates required to achieve a desired surface roughness by a factor of three. The implications of this quantitative surface roughness map over a given processing region are broader than simply suppressing sharkskin to higher output levels or eliminating it entirely at a specific condition, flow rate or pressure drop. Through the use of controlled die heating, the polymer melt extrudate can be processed at a selected operating condition in terms of stress and shear levels, allowing one to ‘dial in’ a specific amplitude and impart a desired functionality to the surface.

The effectiveness of isolated heating at the die wall gives some insight to the mechanism of the sharkskin instability. Our results lend support to the theory that sharkskin originates in the interaction of the polymer with the die wall and local stresses at the die exit. To further quantify this dependence, a local Deborah and Weissenberg number are formed based on the conditions at the capillary die wall:

$$De_{local} = \lambda(T_{die})f, \quad (2)$$

$$Wi_{local} = \lambda(T_{die})\dot{\gamma}_{app}, \quad (3)$$

where f is the frequency of the sharkskin instability. For these calculations, the relaxation time at the wall,

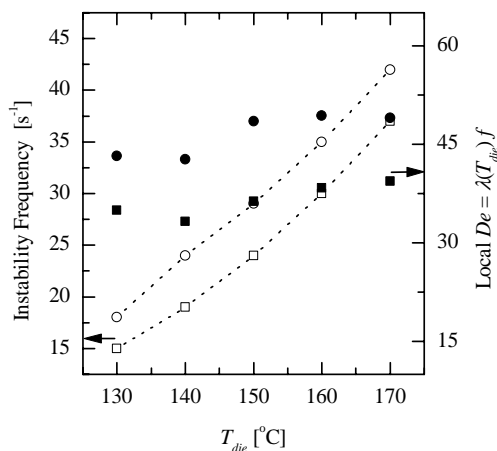


Figure 10: Sharkskin frequency and local Deborah number at die wall as a function of die temperature for fixed apparent shear rate (a vertical slice of Figure 8). The data include: for $\dot{\gamma} = 15s^{-1}$, ‘■’ local De , and ‘□’ frequency; for $\dot{\gamma} = 30s^{-1}$, ‘●’ local De , and ‘○’ frequency.

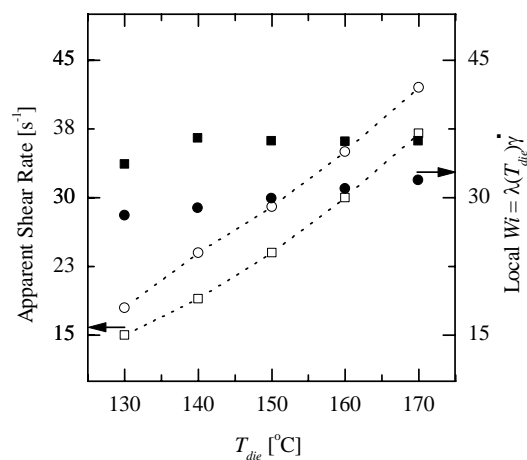


Figure 11: Apparent shear rate and local Weissenberg number at die wall as function of die temperature for a fixed sharkskin amplitude (a horizontal slice of Figure 8). The data include: for $A = 20\mu m$, ‘■’ local Wi , and ‘□’ apparent shear rate; for $A = 30\mu m$, ‘●’ local Wi , and ‘○’ apparent shear rate.

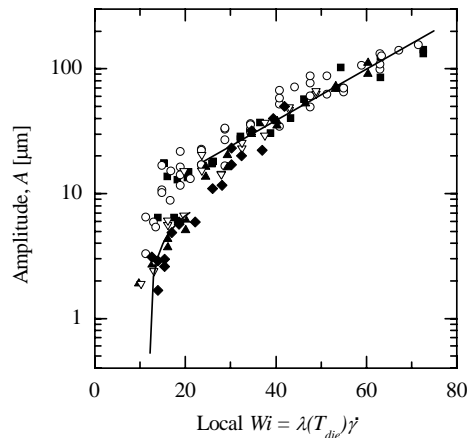


Figure 12: Master curve of all amplitude data at bulk/die temperature conditions from Figure 8 using local Weissenberg number. Fits included for data near and far from onset of sharkskin instability; $A = 2.4(Wi - 12)^{1/2}$ and $A = 5.8e^{0.047Wi}$, respectively.

$\lambda(T_{die})$, was evaluated using the Arrhenius form of the time-temperature superposition shift factor. The Deborah and Weissenberg numbers describe the ratio of the characteristic fluid relaxation time to the characteristic time scale of the flow, and the shear rate, respectively. The two dimensionless quantities also differ in that the Deborah number is used for a time-dependant flow, and Weissenberg for steady flow [25]. In Figure 10, two vertical slices of the data in Figure 8, holding the apparent shear rate constant at $15s^{-1}$ and $30s^{-1}$, are recast in terms of the local Deborah number. As the wall temperature increases, the frequency of the instability increases. When the frequency of the instability is non-dimensionalized by the relaxation time at the die wall to form the local Deborah number, however, the data are found to collapse to a single constant value of $De \sim 38$ for $15s^{-1}$ and $De \sim 50$ for $30s^{-1}$, independent of die temperature. Similarly, if the amplitude is held fixed by taking a horizontal slice of Figure 8, the shear rate required to achieve a given surface roughness can be determined for various die temperatures. The data in Figure

11, for amplitudes of $A = 20\mu m$ and $A = 30\mu m$, show that the apparent shear rate required to achieve a given surface instability amplitude increases with wall temperature. If the shear rate data is non-dimensionalized, the local Weissenberg number is found to remain nearly constant, $Wi \sim 32$ for $A = 20\mu m$ and $Wi \sim 37$ for $A = 30\mu m$, independent of die temperature. From these observations, we can conclude that the sharkskin instability is independent of the viscometric bulk fluid properties and only a function of the rheological properties of the fluid closest to the die wall and the levels of stress due to both viscous and elastic effects resulting from the enormous deformation of the fluid near the stress singularity.

To further demonstrate this conclusion, all of the data from the quantitative map in Figure 8 can be collapsed onto a single master flow curve by plotting the sharkskin amplitude as a function of the local Weissenberg number, shown in Figure 12. Within the limits of experimental error, the data agree very well. The use of this dimensionless quantity now becomes even more insightful. When an exponential fit is applied to the master curve, it becomes clear that there is some critical Weissenberg number ($Wi_{local} \sim 20$) at which there is a transition in the growth rate of the amplitude data. Fitting the data well above the onset conditions ($A > 10\mu m$) for the sharkskin instability gives a scaling of $A = 5.8e^{0.047Wi}$; rewritten in terms of apparent shear rate, this same scaling was also applied to the data in Figure 8 and the results are quite good.

As discussed in the previous section, the absence of hysteresis in the data suggests the transition from a smooth extrudate to the sharkskin instability is a supercritical Hopf bifurcation. An expression for both the amplitude of the surface roughness and the frequency of the instability at Weissenberg numbers close to the onset of the instability can be determined from the following asymptotic results for supercritical Hopf bifurcations [26]

$$A = A_0(Wi_{local} - Wi_{crit})^{1/2}, \quad (4)$$

$$f = c_1 + c_2(Wi_{local} - Wi_{crit})^{1/2}, \quad (5)$$

where Wi_{crit} is the critical Weissenberg number for the onset of the sharkskin instability and A_0 , c_1 , and c_2 are constants. A good fit over all the low Weissenberg number amplitude data ($A < 10\mu m$) in Figure 12 was achieved using Equation (4) and the following parameters: $A_0 = 24\mu m$ and $Wi_{crit} = 12$. These results lend further support to the classification of this instability as supercritical. In addition, this critical Weissenberg number is in good agreement with values reported in the literature [27]. As seen in Figure 12, the initial

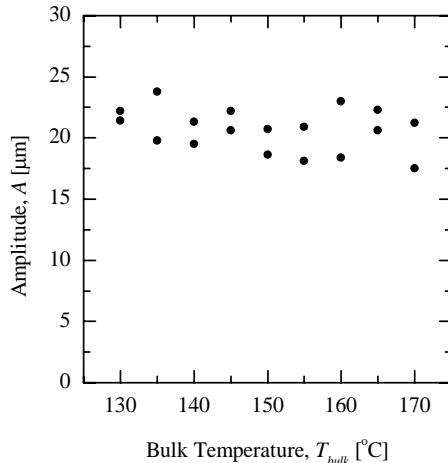


Figure 13: Sharkskin amplitude at constant mass flow rate, $\dot{m} = 0.95$ g/min, as a function of bulk temperature for a fixed wall temperature, $T_{wall} = 150^\circ\text{C}$.

deviations from a smooth extrudate appear to be well described by the linear theory. However, when $Wi_{local} \gg Wi_{crit}$, nonlinear dynamics begin to dominate the flow kinematics and the growth in the amplitude data transitions to the exponential growth regime described previously.

To investigate the role of temperature gradients near the die wall, a final set of experiments were performed. Temperature at the die wall was set to $T_{die} = 150^\circ\text{C}$ and bulk temperature was varied from $T_{bulk} = 130^\circ\text{C}$ to 170°C . Starting with the lowest bulk temperature, output rate was increased to slightly above the point of sharkskin onset. The mass flow rate was recorded and samples were taken for analysis. Pressure was released, bulk temperature increased, and after an equilibration period, the output rate was gradually increased until the same mass output rate was attained at the new temperature conditions. The pressure controlled extruder was adjusted manually for output rates and resulted in an error of approximately 1% about the average.

Figure 13 shows the distribution of data taken at

5°C increments with several samples taken at each increment. Although there is some scatter in the data, which can be attributed to the inherent error in the graphical analysis method at these small amplitudes, the trend in the amplitude is nearly constant with an average value of approximately $A = 20\mu\text{m}$. These experiments demonstrate that the character of the sharkskin amplitude remains constant in the presence of changing temperature gradients and is a function only of the actual temperature at the die wall.

Conclusion

Precise and localized die heating has been shown to suppress the onset of the sharkskin surface instability in the extrusion of LLDPE. Sharkskin has also been quantitatively characterized as a function of the processing conditions showing that the severity of the distortions grows with an exponential trend with increasing apparent shear rate at all die heating conditions. The resulting quantitative processing map for sharkskin amplitude is a useful tool which allows for the precise control of sharkskin surface distortions through the modification of die wall temperature. Analysis of the same quantitative map gives fundamental support to the mechanism of sharkskin being inherent in conditions at the die wall, and nearly independent of conditions in the bulk.

These results have some interesting practical implications to the extrusion of LLDPE and other polymers that exhibit the sharkskin instability. Bulk processing temperatures can be much lower than those needed to suppress the instability. The heating of a very small portion of the die at the exit provides the same benefit as processing the entire bulk at that higher temperature. Bulk processes can be cooler and more energy efficient, while cooling times of the polymer melt extrudate are minimized. Precise control of sharkskin as alluded to in the preceding experimental results leads to future theoretical applications such as the extrusion of products with specifically designed or even varying surface roughness. In film blowing or sheet extrusion, inner and outer dies could produce surfaces smooth on one side and rough on the other. On a qualitative level, it has already been shown that temperature gradients between the inner and outer die lips in a film blowing application produce smooth and sharkskin surfaces on the respective surfaces of a bubble [28]. Further development of temperature control systems could result in dies that would respond quickly and could pattern surfaces as they were extruded.

References

- [1] Petrie, C. J. S., and Denn, M. M., "Instabilities in Polymer Processing," *AIChE J.*, **22** (1976) 209-236.
- [2] Denn, M. M., "Extrusion instabilities and wall slip," *Annu. Rev. Fluid Mech.*, **33** (2001) 265-287.
- [3] Howells, E. R., and Benbow, J. J., "Flow defects in polymer melts," *Trans. J. Plast. Inst.*, **30** (1962) 240-253.
- [4] Tordella, J. P., "Unstable flow of molten polymers: A second site of melt fracture," *J. Appl. Polymer Sci.*, **7** (1963) 215-229.
- [5] Larson, R. G., "Instabilities in viscoelastic flows," *Rheol. Acta*, **31** (1992) 213-263.
- [6] Cogswell, F. N., "Stretching flow instabilities at the exits of extrusion dies," *J. Non-Newtonian Fluid Mech.*, **2** (1977) 37-47.
- [7] Barone, J. R., Plucktaveesak, N., and Wang, S. Q., "Interfacial molecular instability mechanism for sharkskin phenomenon in capillary extrusion of linear polyethylenes," *J. Rheol.*, **42** (1998) 813-832.
- [8] Mackley, M., Rutgers, R., and Gilbert, D., "Surface instabilities during the extrusion of linear low density polyethylene," *J. Non-Newtonian Fluid Mech.*, **76** (1998) 281-297.
- [9] Mhetar, V., and Archer, L. A., "Slip in entangled polymer melts. 1. General features," *Macromolecules*, **31** (1998) 8607-8616.
- [10] Dhori, P. K., Jeyaseelan, R. S., Giacomini, A. J., and Slattery, J. C., "Common line motion III: implication in polymer extrusion," *J. Non-Newtonian Fluid Mech.*, **71** (1997) 231-243.
- [11] Migler, K. B., Lavalee, C., Dillon, M. P., Woods, S. S., and Gettinger, C. L., "Visualizing the elimination of sharkskin through fluoropolymer additives: Coating and polymer-polymer slippage," *J. Rheol.*, **45** (2001) 565-581.
- [12] Inn, Y. W., Fisher, R. J., and Shaw, M. T., "Visual observation of development of sharkskin melt fracture in polybutadiene extrusion," *Rheol. Acta*, **37** (1998) 573-582.
- [13] Piau, J.-M., Kissi, N. E., Toussant, F., and Mezghani, A., "Distortion of polymer melt extrudates and their elimination using slippery surfaces," *Rheol. Acta*, **34** (1995) 40-57.
- [14] Ramamurthy, A. V., "Wall slip in viscous fluids and influence of materials of construction," *J. Rheol.*, **30** (1986) 337-357.
- [15] Ghanta, V. G., Riise, B. L., and Denn, M. M., "Disappearance of extrusion instabilities in brass capillary dies," *J. Rheol.*, **43** (1998) 435-442.
- [16] Perez-Gonzalez, J., and Denn, M. M., "Flow enhancement in the continuous extrusion of linear low-density polyethylene," *Ind. Eng. Chem. Res.*, **40** (2001) 4309-4316.
- [17] Chung, C. I., *Extrusion of Polymers: Theory and Practice*, Carl Hanser Verlag, Munich, 2000.
- [18] Michaeli, W., *Extrusion Dies: Design and Engineering Computations*, Carl Hanser Verlag / Macmillan Publishing Co., Munich, 1984.
- [19] Cogswell, F. N., "A method for reducing sharkskin on extruded polymeric material," *British Patent #1 441 586*, (1976).
- [20] Santamaria, A., Fernandez, M., Sanz, E., Lafuente, P., and Munoz-Escalona, A., "Postponing sharkskin of metallocene polyethylenes at low temperatures: the effect of molecular parameters," *Polymer*, **44** (2003) 2473-2480.
- [21] Bird, R. B., Armstrong, B. C., and Hassager, O., *Dynamics of Polymeric Liquids: Volume 1 Fluid Mechanics*, John Wiley & Sons, New York, 1987.
- [22] Winter, H. H., "Viscous dissipation in shear flows of molten polymers," *Adv. Heat Transfer*, **13** (1977) 205-267.
- [23] Coppeta, J., and Rogers, C., "Dual emission laser induced fluorescence for direct planar scalar behavior measurements," *Exp. Fluids*, **25** (1998) 1-15.
- [24] Pudjijanto, S., and Denn, M. M., "A stable "island" in the slip-stick region of linear low-density polyethylene," *J. Rheol.*, **38** (1994) 1735-1744.
- [25] Morrison, F. A., *Understanding Rheology*, Oxford University Press, New York, 2001.
- [26] Iooss, G., and Joseph, D., *Elementary Stability and Bifurcation Theory*, Springer, New York, 1980.
- [27] Meulenbroek, B., Storm, C., Bertola, V., Wagner, C., Bonn, D., and Saarloos, W. v., "Intrinsic route to melt fracture in polymer extrusion: A weakly nonlinear subcritical instability in viscoelastic Poiseuille flow," *Physical Review Letters*, **90** (2003) 024502(4).
- [28] Rutgers, R., Clemeur, N., and Husny, J., "The prediction of sharkskin instability observed during film blowing," *International Polymer Processing*, **17** (2002) 214-222.